# Supplementary Material

May 11, 2023

## 1 Coupled Layered Intrusion-Melt Model

In this section, we describe the coupled layered intrusion-melt model referred to in the main text. The setup is shown schematically in figure 1.

### 1.1 Layered Intrusion Model

The layered intrusion model is as described by Robel et al., 2022 and Wilson et al., 2020, albeit with a variable channel thickness. The 'along grounding zone' (transverse) average behaviour of the subglacial hydrological system is considered as a two layer system in which cold, fresh subglacial discharge from upstream of the grounding zone is underlain by warm, saline ocean water. These two layers are treated as immiscible (except for the exchange of heat, see below). The grounding zone is inclined at an angle $\theta$ to the horizontal, along which the $x$-axis is aligned. The layer-averaged velocity and thickness of the warm and cold layers are denoted by $u_i(x,t)$ and $h_i(x,t)$ for $i = 1,2$, respectively (supplementary figure 1). Far upstream of the grounding zone, the subglacial network is assumed to have an average thickness $H_\infty$ and fresh water flow velocity $U_\infty$. Conservation of mass of the two layers is expressed by

$$\frac{\partial h_1}{\partial t} + \frac{\partial}{\partial x}(u_1 h_1) = 0, \tag{1}$$

$$\frac{\partial h_2}{\partial t} + \frac{\partial}{\partial x}(u_2 h_2) = 0, \tag{2}$$

where $h = h_1 + h_2$ is the total channel thickness, and $q_i = h_i u_i$, $i = 1,2$ is the flux in layer $i$. Note that (1)–(2) results from assuming negligible fresh water input via melting into the fresh water layer. Although melting is important in altering the thickness of the subglacial channel, the water input due to this melting is insignificant compared to the flux of water from upstream. For example, a typical value of the upstream subglacial flux is $U_\infty H_\infty \approx 10^{-2}$ m$^2$ s$^{-1}$, while the total input from melting is on the order of $\int \dot{m} \approx 10^{-4}$m$^2$ s$^{-1}$, where the integral is taken over the horizontal lengthscale. (More generally, taking the horizontal lengthscale $H_\infty/c_d$ as identified below, the ratio between upstream subglacial flux and total input from melting is on the order of $\mathrm{St}c/L\Delta T/c_d \sim 10^{-2}$.)

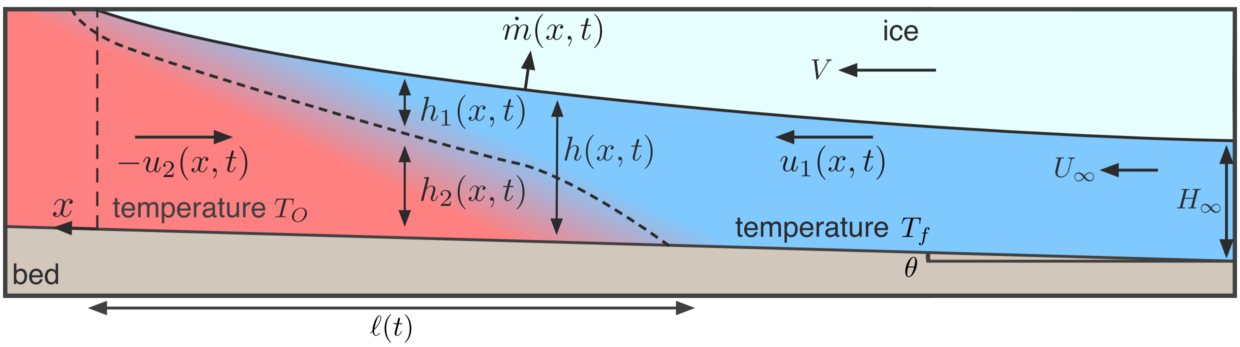


**Supplementary figure 1:** Schematic diagram of the the grounding zone model: warm, salty water of temperature $T_O$ (red) is overlain by cold, fresh water (blue) at the local temperature $T_f$. The grey dashed curve indicates an approximation to the interface between the layers. Note that the vertical scale has been exaggerated for clarity.

Momentum conservation in each layer requires

$$\frac{\partial u_1}{\partial t} + u_1\frac{\partial u_1}{\partial x} + \frac{1}{\rho}\frac{\partial P}{\partial x} + \frac{c_i|u_1-u_2|(u_1-u_2)}{h_1} + \frac{c_d u_1^2}{h_1} = 0, \tag{3}$$

$$\frac{\partial u_2}{\partial t} + u_2\frac{\partial u_2}{\partial x} + \frac{1}{\rho}\frac{\partial P}{\partial x} - \frac{c_i|u_1-u_2|(u_1-u_2)}{h_2} + \frac{c_d u_2^2}{h_2} + g'\left(\frac{\partial h_2}{\partial x} + \tan\theta\right) = 0. \tag{4}$$

where $P$ is the barotropic pressure within the channel, $c_i$ is the coefficient of interfacial drag between the two layers, and $c_d$ is the coefficient of wall drag. These two drag coefficients parametrize the behaviour in the transverse (along grounding line) direction, with high values of $c_d$ corresponding to strong wall-fluid interactions (and vice versa for low $c_d$) and high values of $c_i$ corresponding to strong resistance between the layers. In (3)–(4), $g' = g\Delta\rho/\rho_0$ is the reduced gravity, with $g$ the gravitational acceleration, $\Delta\rho$ the density difference between the two layers, and $\rho_0$ a reference density. We assume that the density difference between the two layers is constant, which is approximately equivalent to assuming that there is no salinity exchange between the layers (density is subglacial systems is set primarily by salinity (Hewitt, 2020)).

For a given channel thickness $h(x,t)$, the system (1)–(4), alongside the geometric constraint $h = h_1 + h_2$, are a system of five equations for the five unknowns $u_1$, $u_2$, $h_1$, $h_2$, and $P$. This system is closed with boundary conditions: firstly, the thickness and velocity of the upstream subglacial hydrological network are prescribed:

$$u_1 = U_\infty, \qquad h_1 = H_\infty \qquad \text{as } x \to -\infty. \tag{5}$$

Secondly, the upper-layer must be at the subcritical-to-supercritical transition at the channel entrance (Wilson et al., 2020)

$$\frac{u_1}{\sqrt{g'h_1}} = 1 \qquad \text{at } x = 0. \tag{6}$$

The boundary condition (6) arises because the freshwater flow becomes unconfined as it leaves the region and hence its behaviour is expected to transition from subcritical to supercritical there (see Wilson et al., 2020 for a full description of this boundary condition).

Following Wilson et al., 2020 and Robel et al., 2022, the system (1)–(4) is simplified by making the assumption that the flow in both layers flow is steady (i.e. all time derivatives in (1)–(4) are ignore). Unlike the models of Wilson et al., 2020 and Robel et al., 2022, our model has another timescale in it, namely that on which the confining channel geometry changes. The relevant timescale for flow in the channel (of given width) to reach equilibrium is the advective timescale $\mathcal{L}/u_\infty$, where $\mathcal{L} = H_\infty/c_d$ is the lengthscale of the channel, while the timescale over which the geometry evolves (see §1.3 below) is the ice advection timescale $\mathcal{L}/V$. This latter timescale is typically $10^4$ times larger than the former, so it is reasonable to treat the hydraulic equations (3)–(3) as quasi-steady. A result of assuming this quasi-steady state is that the average velocity of the lower layer must be zero ($u_2 = 0$). (In fact, there is likely some recirculation of fluid within the lower layer – inwards along the bottom and outwards along the top – but there is no net horizontal flow.)

Noting that the flux of fluid in the fresh layer is constant, $q_1 = u_1 u_1 = U_\infty H_\infty = q_\infty$) and taking the difference of(3)–(4), we obtain a single ODE for $h_1$:

$$\left[\left(\frac{U_\infty}{\sqrt{g'h_1}}\right)^2 - 1\right]\frac{\partial h_1}{\partial x} = \left(\frac{U_\infty}{\sqrt{g'h_1}}\right)^2\left(c_d + c_i\frac{h}{h-h_1}\right) - \left(\tan\theta + \frac{\partial h}{\partial x}\right). \tag{7}$$

## 1.2 Melting and Channel Evolution

Flow through the grounding zone feeds back on the channel shape via melting of the upper surface at a rate $\dot{m}(x,t)$. Since grounding zones are long and thin, this melt rate can reasonably be assumed to apply perpendicular to the basal slope.

We apply the so-called 'two equation formulation' for melting. The two equations refer to a liquidus condition and approximate heat balance,

$$T_f(S, z_b) = T_{\text{ref}} + \lambda z_b - \Gamma S, \quad \dot{m}\left\{L + c_i\left[T_f(S,z_b) - T_i\right]\right\} = \text{St}u^* c\left[T - T_f(S,z_b)\right]. \tag{8}$$

Here $T_{\text{ref}} = 8.32 \times 10^{-2}$ °C is a reference temperature, $\lambda = 7.61 \times 10^{-4}$ °C m$^{-1}$ is the liquidus slope with depth, $\Gamma = 5.73 \times 10^{-2}$ °C is the liquidus slope with salinity, $z_b$ is the local depth, $L = 3.35 \times 10^5$ J kg$^{-1}$ is the latent heat of fusion of seawater, $c_i = 2.009 \times 10^3$ J kg °C$^{-1}$ is the specific heat capacity of ice, $T_i$ is the internal ice temperature, St is a combined Stanton number, $u^*$ is the velocity outside a viscous boundary layer adjacent to the ice-ocean interface, $c = 3.974 \times 10^3$ J kg °C$^{-1}$ is the specific heat capacity of water, and $T$ and $S$ are the temperature and salinity outside the viscous boundary layer, respectively. (Values quoted here are standard values, assumed constant, from Jenkins et al., 2010 and Hewitt, 2020.)

Since the local freezing temperature and internal ice temperature are within a few degrees of each other, then $|T_f(S, z_b) - T_i| \ll L/c_i$ and the second of (8) can be approximated by

$$L\dot{m} = \mathrm{St} c u^* \tau, \tag{9}$$

where $\tau = T - T_f(S, z_b)$ is the local thermal forcing. By dividing both sides of (9) by $L$, we obtain equation (2) in the methods section of the main text.

We take the freshwater layer velocity, which is the layer adjacent to the ice-oceean interface, as the boundary layer velocity, i.e. $u^* = u_1$.

In general, the local freezing temperature $T_f(S, z_b)$ is determined from the first of (8) using the local salinity and grounding line depth; however since $T_f$ has only a very weak dependence on salinity, and vertical variations are relatively small, it is reasonable to assume that $T_f$ is constant.

We take a simple model for the channel temperature, assuming that the temperature in the channel is the depth-weighted average of the layer temperatures:

$$T = \phi T_d + (1 - \phi) T_O, \quad \phi = \frac{h_1}{h}, \tag{10}$$

where $T_d$ is the temperature of the subglacial discharge (assumed to be at the local freezing temperature, i.e. $T_d = T_f$), and $T_O$ is the ocean temperature.

To close the model, we must describe how the channel geometry responds to melting. With the assumption that the ice above the channel has constant velocity $V$ (a reasonable assumption given the long, $\mathcal{O}(10\text{ s})$ kms on which ice sheet velocities vary), the kinematic boundary condition on the upper surface requires:

$$\frac{\partial h}{\partial t} + V \frac{\partial h}{\partial x} = \dot{m}. \tag{11}$$

As initial conditions, we take a configuration of parallel channel walls: $h(x, t = 0) = 1$, which is the configuration of Robel et al., 2022 and Wilson et al., 2020. We are primarily interested in the final configuration; as we show in § 2, the steady solution, should it exist, is unique and therefore independent of the initial condition used.

With an initial condition specified, the timestepping process is as follows: for the given channel thickness $h(x, t)$, we use equation (7) to determine the freshwater water layer thickness $h_1$ (at the first timestep, when the channel walls are parallel, this is the solution described by Robel et al., 2022 and Wilson et al., 2020) and thus the thermal driving from (10). The freshwater layer velocity is then be determined via conservation of mass ($h_1 u_1 = H_\infty U_\infty$) and the melt determined using (9). The thickness is then be updated using (11), and the procedure repeated.

## 1.3 Non-dimensionalization

The problem (7), (9), (11) is non-dimensionalized by introducing dimensionless variables (denoted with hats):

$$\hat{h}_1 = \frac{h_1}{H_\infty}, \qquad \hat{h} = \frac{h}{H_\infty}, \qquad \hat{x} = \frac{c_d\, x}{H_\infty}, \qquad \hat{t} = \frac{t}{\mathcal{T}}. \tag{12}$$

The scales introduced are based on a horizontal lengthscale $H_\infty/c_d$ and the melting timescale $\mathcal{T} = H_\infty L/(U_\infty \mathrm{St} c \Delta T)$.

After inserting dimensionless variables (12), the channel flow equation (7) becomes

$$\left(\frac{F^2}{\hat{h}_1^3} - 1\right) \frac{\partial \hat{h}_1}{\partial \hat{x}} = \frac{F^2}{\hat{h}_1^3} \left(1 + C \frac{h}{\hat{h} - \hat{h}_1}\right) - \left(S + \frac{\partial \hat{h}}{\partial \hat{x}}\right), \tag{13}$$

where $F = U_\infty / \sqrt{g' H_\infty}$ is the upstream Froude number, $S = \tan\theta / c_d$ is the rescaled bed slope, and $C = c_i / c_d$ is a rescaled drag coefficient.

After combining the melt model (9) and the kinematic condition (11), and inserting dimensionless variables (12), we obtain

$$\frac{\partial \hat{h}}{\partial \hat{t}} + \frac{1}{M} \frac{\partial \hat{h}}{\partial \hat{x}} = \frac{1}{\hat{h}_1} \left(1 - \frac{\hat{h}_1}{\hat{h}}\right) \tag{14}$$

where

$$M = \frac{U_\infty}{V} \frac{\mathrm{St}}{C_d} \frac{\Delta T}{L/c} \tag{15}$$

is the dimensionless melt parameter.

The dimensionless boundary and initial conditions are

$$\hat{h}_1(x=0,t)^{3/2} = F^{2/3} \tag{16}$$

and

$$\hat{h}(x,t=0) = 1. \tag{17}$$

The dimensionless intrusion length, denoted $\hat{\ell}(\hat{t})$, is determined by the condition that $\hat{h} = \hat{h}_1$ at $\hat{x} = -\hat{\ell}(\hat{t})$. The final intrusion length, which is shown in figures 3–4 of the main text, is $L = \lim_{\hat{t}\to\infty} \hat{\ell}$.

# 2 Steady Intrusion Length

In this section, we describe the procedure for determining the steady intrusion length $L$. Note that in this section, all variables are assumed dimensionless and hats are dropped.

## 2.1 Steady Intrusion Problem

To determine the steady intrusion length $L$ for a given set of parameters $(F,\ C,\ S,\ M)$, we consider the steady form of the coupled layered intrusion-melt equations (13)–(14), which read

$$\left(\frac{F^2}{h_1^3} - 1\right)\frac{\mathrm{d}h_1}{\mathrm{d}x} = \frac{F^2}{h_1^3}\left(1 + C\frac{h}{h-h_1}\right) - \left(S + \frac{\mathrm{d}h}{\mathrm{d}x}\right), \tag{18}$$

$$\frac{1}{M}\frac{\partial h}{\partial x} = \frac{1}{h_1}\left(1 - \frac{h_1}{h}\right). \tag{19}$$

If a steady solution with a bounded intrusion exists, it will necessarily have $h = h_1 = 1$ at $x = L$ and $h_1 = F^{2/3}$ at $x = 0$.

The idea is as follows: we begin by specifying an arbitrary finite interval $[x_l, x_u]$, where $x_u - x_l \gg 1$ and then integrate (18)–(19) forwards in $x$ from $x = x_l$ towards $x = x_u$. Should the solution reach the sub-supercritical transition threshold (16) at a point $x = x_s \in [x_l, x_u]$, then the steady intrusion length is $L = x_s - x_l$. However, if the solution does not reach (16), there is no steady solution with a bounded intrusion length. The specific values $x_u$ and $x_l$ are arbitrary because the problem (18)–(19) is translationally invariant. In the results shown here, we take $x_u - x_l = 10^5$.

To avoid a singularity in the interfacial drag term that appears in the momentum equation (19) at the nose of the intrusion (where $h_1 = h$), we integrate (18)–(19) using a perturbed initial condition, based on an asymptotic expansion of the local solution,

$$h = 1 + \frac{2M}{3}\left(\frac{2CF^2}{1-F^2}\right)^{1/2} x_\epsilon^{3/2}, \tag{20}$$

$$h_1 = 1 - \left(\frac{2CF^2}{1-F^2}\right)^{1/2} x_\epsilon^{1/2}, \tag{21}$$

at $x = x_l + x_\epsilon$ where $x_\epsilon \ll 1$ (in the results shown here and in the main text, we used $x_\epsilon = 10^{-3}$, but found that results are insensitive to this value provided that $x_\epsilon \ll 1$).

In figure 2, we show the solution to (18)-(21) using the parameter values used to generate figure 2 of the main text and $x_l = 10^5$). This demonstrates the procedure: for the smaller value of $M$ ($M = 0.27$, left panels in figure 2), the solution $h_1$ decreases monotonically from $h_1 = 1$ at $x = x_l$ to $h_1 = F^{2/3}$, which is attained at $x = x_s \approx 4$. Thus, this parameter set corresponds to a bounded intrusion, with a dimensional intrusion length of approximately 110m. For the larger value of $M$ ($M = 0.3$, right panels in figure 2), $h_1$ initially decreases (inset in figure 2b) before reaching a local minimum at a value larger than $F^{2/3}$ and increasing monotonically thereafter. The termination value $h_1 = F^{2/3}$ is never attained.

This behaviour is generic: for $M < M_c$, the solution for $h_1$ always heads monotonically towards $h_1 = F^{2/3}$, attaining it in a finite distance, while for $M > M_c$, the solution attains a local minimum beyond which it increases without bound. It is possible to show – although it does not provide insight and is therefore not included here – that any solution of (18)–(19) has a unique local minimum and thus, if a local minimum with $h_1 > F^{2/3}$ is attained, the solution will never attain $h_1 = F^{2/3}$. This confirms that for $M > M_c$, no bounded, steady intrusion exists.

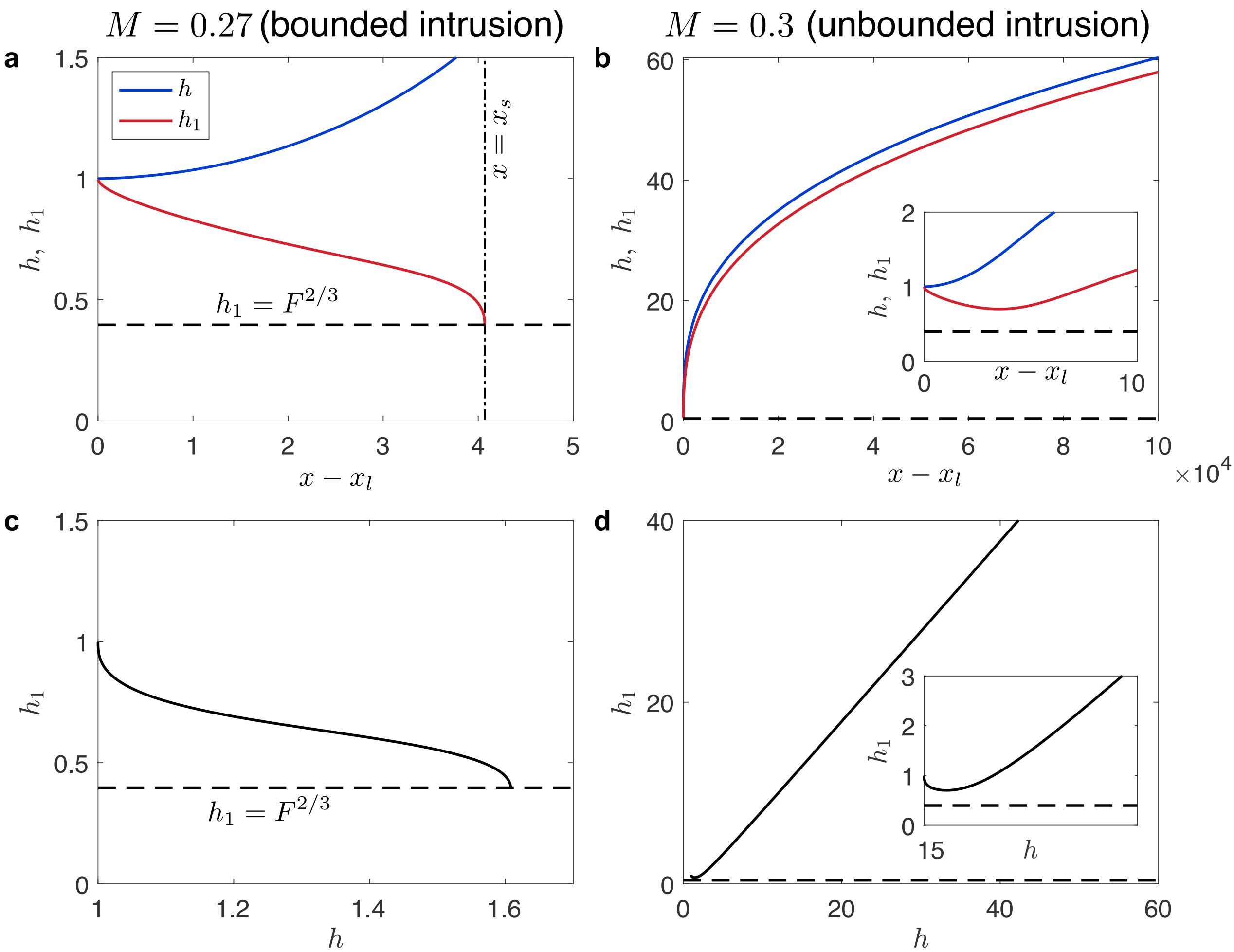


**Supplementary figure 2:** Numerical solutions of the steady coupled intrusion-melt equations (18)–(19). Solutions are shown in (a–b) $(x - x_l, h)$ space and (c–d) $(h, h_1)$ space. In each panel, the horizontal dashed line indicates the boundary condition $h_1 = F^{2/3}$, at which the solution would terminate, if it was attained. Results are shown for $M = 0.27$ (left-hand panels) and $M = 0.3$ (right-hand panels), corresponding to ocean temperatures of 1.8°C and 2.0°C, respectively. These solutions are generated using a flat bed ($S = 0$), a fairly inefficient drainage system ($F = 0.25$), and $C = 0.1$. In (b) and (d), insets are as in the main panel, but zoomed in around the origin.

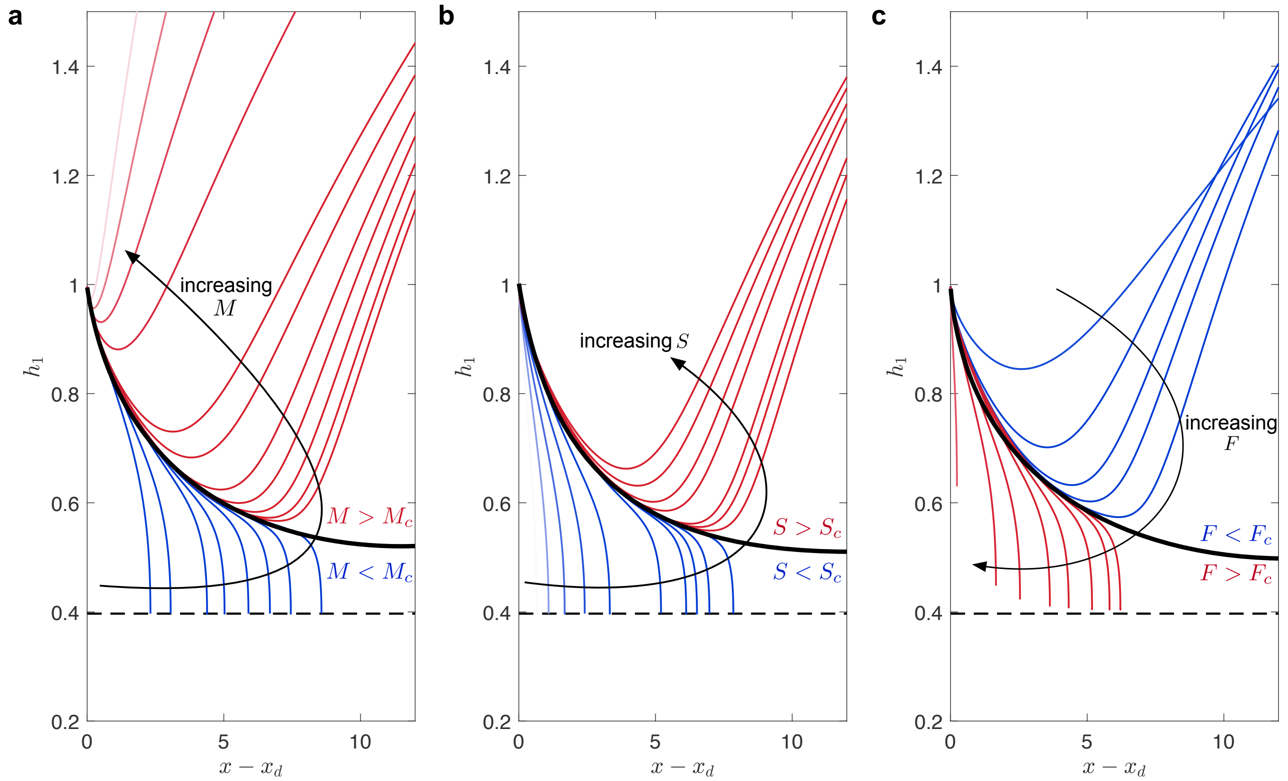


**Supplementary figure 3: Determining critical parameters for intrusion.** Panels show $h_1$ as a function of $x - x_d$ for different values of (a) $M$, (b) $S$ values and (c) $F$. In each case, red (blue, respectively) curves indicate solution trajectories when the parameter is above (below) its continuous intrusion threshold, indicated with a subscript $c$ (i.e. $M_c$, $S_c$, and $F_c$). Black curves indicate the solution trajectory with parameter values at the threshold.

## 2.2 Bisection algorithm for $M_c$

To determine the critical melt parameter $M_c$ shown as the boundary between green and blue sections of figure 3 of the main text, we apply a bisection method. For a given $(F, S, C)$, we first determine an upper $M_c^u$ and lower $M_c^l$ bound on $M_c$, determined as any value which result in unbounded and bounded intrusion, respectively. We then apply a standard bisection procedure: at each step, we take a candidate melt parameter as the mean of the current upper and lower bound value. The steady equations (18)–(19) are then solved using this value of $M$; if this value corresponds to unbounded (bounded, respectively) intrusion, it replaces the upper (lower) bound. This procedure is repeated until the difference between the upper and lower bounds is below a predetermined threshold (in those results shown here, this is $10^{-3}$). Examples of the solutions $h_1$ generated during this procedure are shown in supplementary figure 3a.

The same procedure outlined in this section is applied to determine the critical slope $S_c$ and critical Froude number $F_c$ (noting that unbounded intrusion occurs for $F < F_c$ and thus the bisection algorithm must be adjusted accordingly). Examples $h_1$ generated during this procedure are shown in supplementary figure 3b (for $S_c$) and figure 3c (for $F_c$).

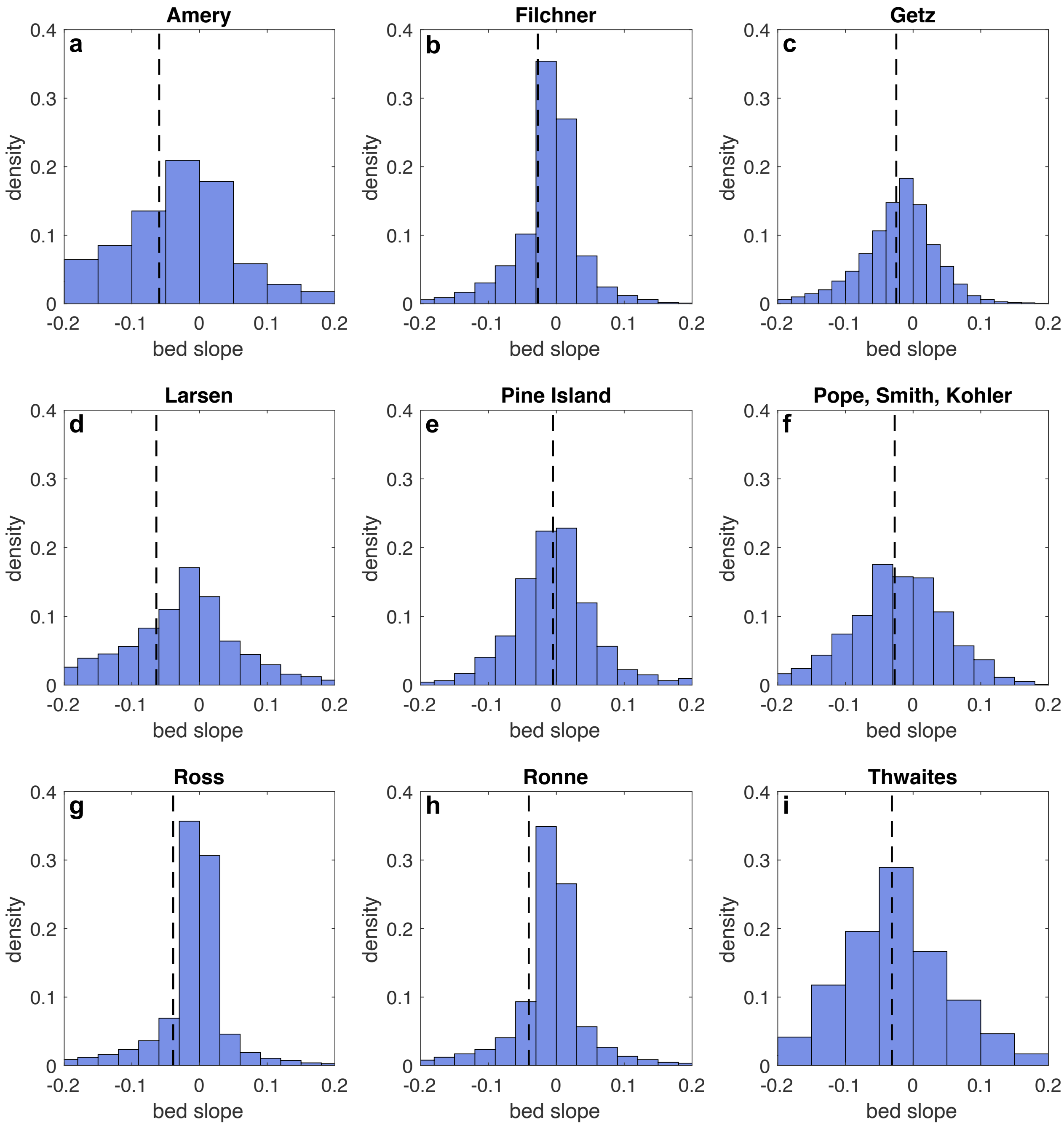


**Supplementary figure 4:** Histograms of grounding line slope for selected Antarctic glaciers. In each panel, the black dashed line indicates the mean of the data showed therein.

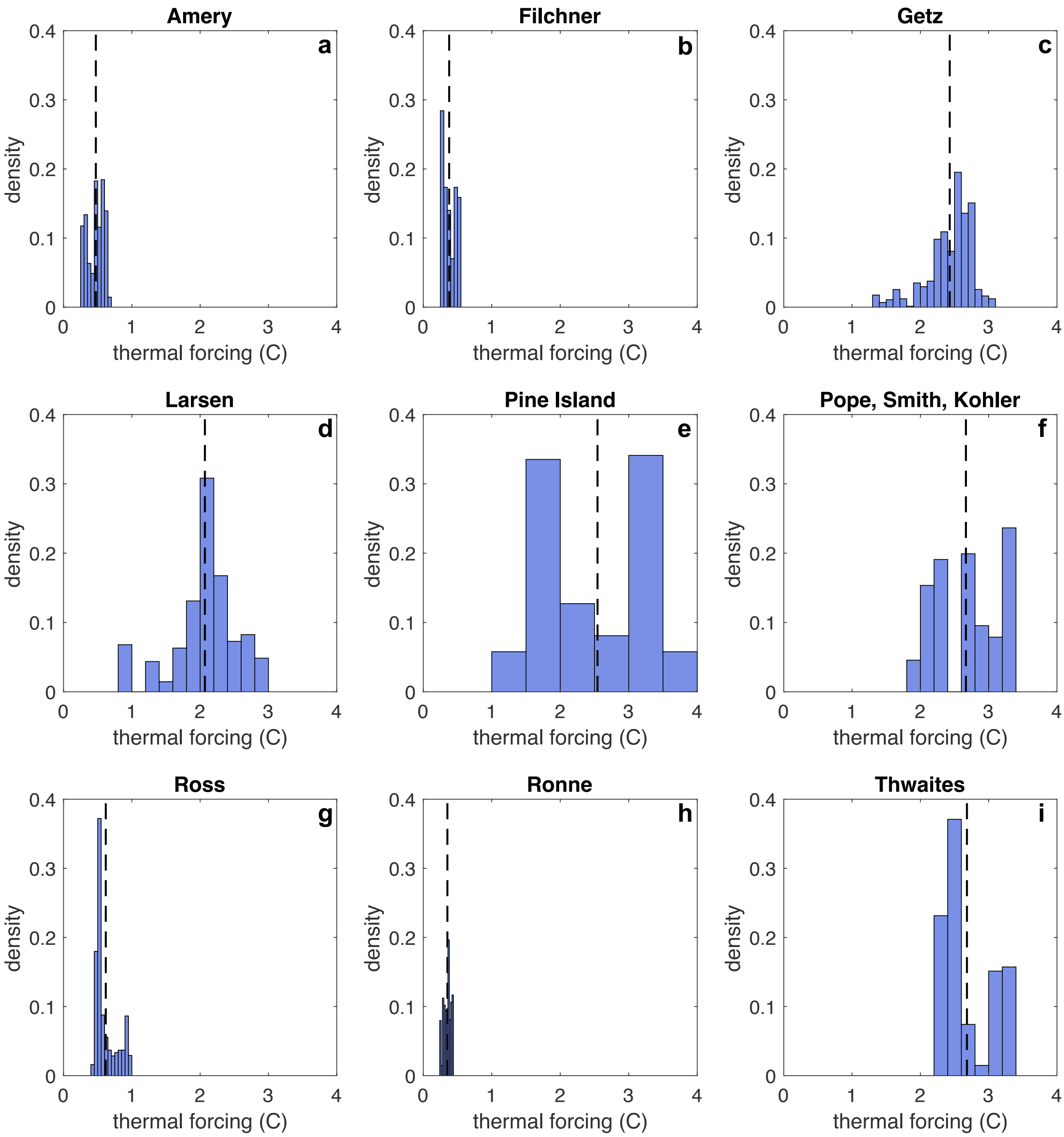


**Supplementary figure 5:** Histograms of thermal driving for selected Antarctic glaciers. In each panel, the black dashed line indicates the mean of the data showed therein.

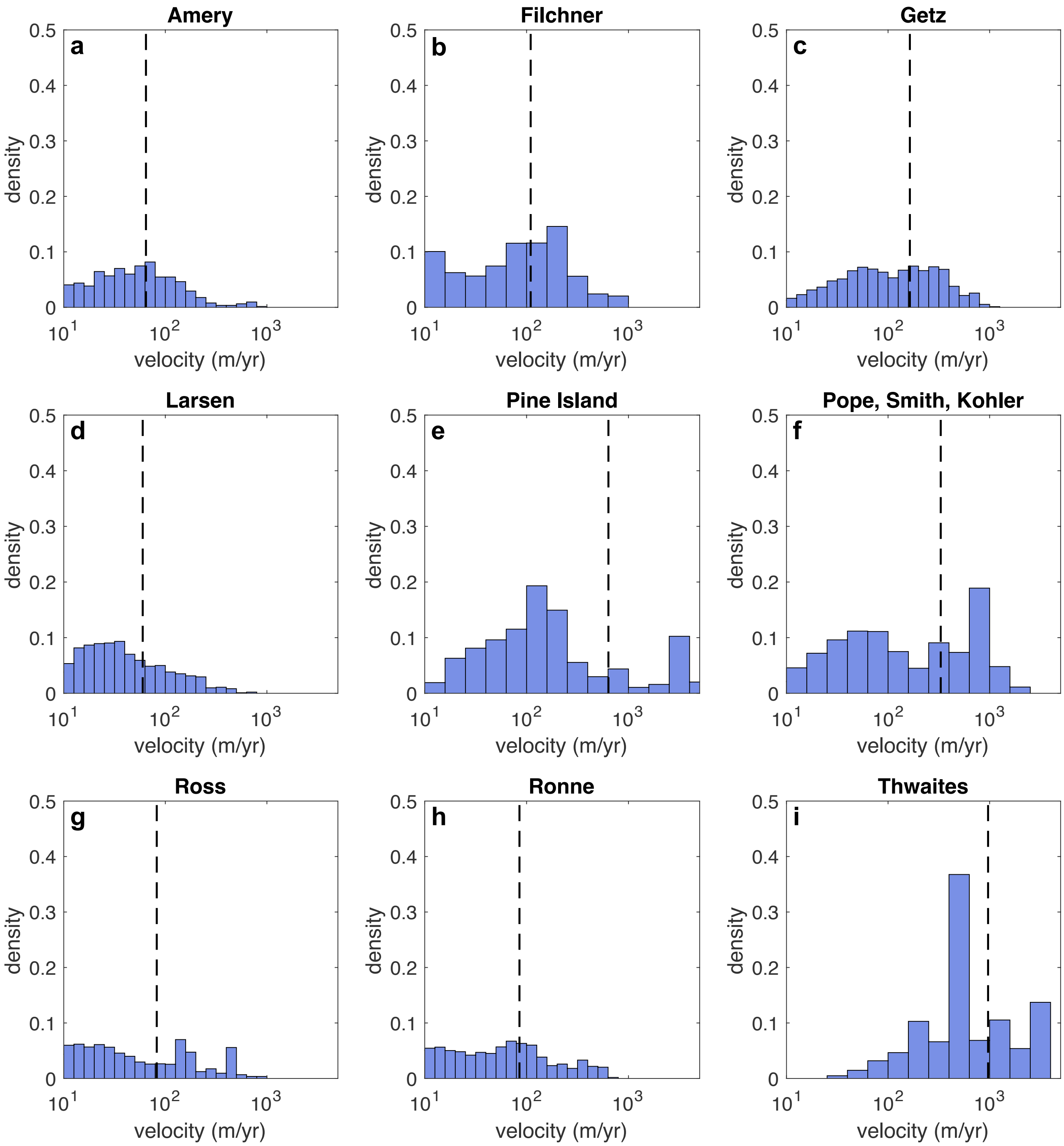


**Supplementary figure 6:** Histograms of grounding line velocity for selected Antarctic glaciers. In each panel, the black dashed line indicates the mean of the data showed therein.

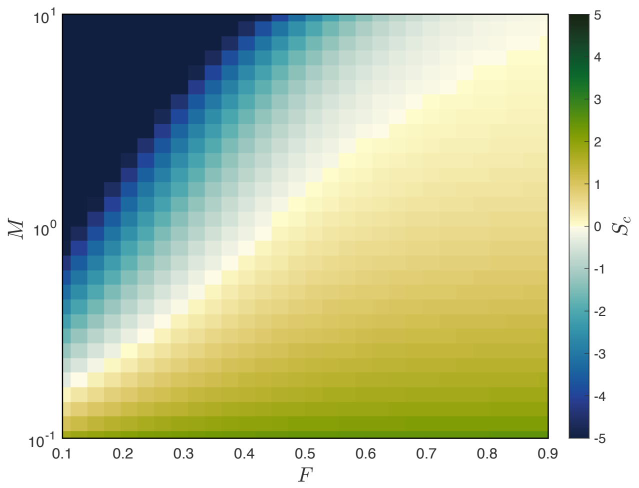


**Supplementary figure 7:** Critical slope for intrusion $S_c$ as a function of dimensionless hydrological network efficiency $F$ and melt parameter $M$.